Developing an Integrated Imaging System for the 70 nm Node Using High Numerical Aperture ArF Lithography

John S. Petersen[1], James Beach[2], David J. Gerold[1], Mark J. Maslow[1]

1. Petersen Advanced Lithography, Inc, 12325 Hymeadow Drive, Suite 2-201 Austin, TX 78750 USA
2. International SEMATECH, 2706 Montopolis Drive, Austin, TX 78741 USA
email: jpetersen@advlitho.com

At its conception, 193 nm lithography was thought to be the best way to take optical lithography to the 180 nm node. It was expected that 193 nm could support the now-defunct 160 nm node before optical lithography would have to yield to an undetermined non-optical solution. Today, 193 nm must compete with 248 nm for the 130 nm node and is expected to support lithography until it is replaced by 157 nm at the 70 nm node. Given the challenges facing 157 nm, it is likely that lithographers will attempt to extend the utility of 193 nm to its theoretical limits.

When attempting a process with k_1 below 0.3, one cannot consider the resist, illumination and mask systems separately. We will take an integrated approach utilizing a combination of advanced phase shift, OPC and illumination techniques in an attempt to demonstrate the feasibility of using 0.75 NA 193 nm lithography to support the 70 nm node. Simulated process windows, profiles and focus effects will be compared to modeling predictions for both line/space and contact features. Special emphasis is placed on SRAM cell designs, primarily the gate level.

Keywords: microlithography, advanced imaging, phase shift mask, PSM, Sidewall chrome alternating aperture mask, SCAA mask, SRAM cell, optical proximity correction, OPC, illumination, numerical aperture, off-axis illumination, OAI

Introduction

Optical lithography evolves, continually making it possible to image ever smaller features that the designers can in turn use to increase device density. Through simulations, this work describes the different image integration issues needed to attain the 70nm technology node. The targets for this work were to use 193nm, 0.75NA exposure to produce 140nm pitch with 45nm and 70nm gates, and 160nm pitch with 45nm gates. Also examined are the device-like structures and contacts 6T (transistor) SRAM, 4T Nand-gates and 2T features. To accomplish this, two imaging techniques are studied. The first is the strong phase-shifted dark field alternating phase-shift mask technique,[1, 2, 3] using highly coherent, partially coherent illumination. The second gate imaging technique uses chromeless phase-shift lithography[4] in its simplest shifter-shutter form,[5, 6] and extreme off-axis dipole illumination[7]. For contacts, attenuated PSM with extreme off-axis cross-quadrupole illumination was studied. The geometry of the cross-quad illuminator is best suited for imaging where diffraction patterns are spread too far apart in the lens for conventional 45° quadrupoles to work and where other techniques like annular and dipole illumination are too weak for production worthiness.

Additionally, the oblique interference angles of the diffraction patterns produced by low k1 imaging with high NA requires that the optical stack of which the resist is part must be optimized. This is all part of what is needed to design an integrated imaging system. This integration has historically occurred in the factory, developed by the photolithographers, but today, since it will take new designs and capabilities, needs to occur in the infrastructure if it is to be truly successful.[8]

This work examines the type of alternating PSM needed for the 70nm node, compares strong to weak PSM techniques and examines what illuminator is needed for each. Resists are not examined nor is the optical stack optimized. The simulators used are PROLITH™ from KLA-Tencor and EM-Suite's TEMPESTpr from Panoramic Technology.

Strong PSM On-axis Illumination

The exposure tool for this work has a maximum numerical aperture, 0.75, needed since in sigma space (the Fourier plane) places the diffraction orders at:

$$\sigma_{\pm 1st\text{-}order} = \lambda \cdot (2 \cdot Pitch \cdot NA)^{-1} = 193nm \cdot (2 \cdot 140nm \cdot 0.75)^{-1} = 0.92$$

which places the diffraction orders at the very edge of the pupil. For strong phase shifting, the best results occur with a high degree of coherence. Historically, a value of 0.3 to 0.45 is the typical sigma value chosen for strong PSM applications. However, it has been observed that depth of focus (DoF) decreases with increasing numerical aperture, which for the casual lithographer is assumed to be related to the Raleigh criterion $= DoF = k_2 \, \lambda/NA^2$. However, this relationship does not hold for two-beam imaging, which is in phase as long as spatial and temporal coherence are maintained. In addition, the loss of DoF shown in Figure 1 shows for the same diffraction pattern, in this case a 120nm equal line-space, that DoF decreases with increasing NA. The reason for this lies in the definition of partial coherence,

$$\sigma = \sin(\text{illuminator half cone angle}) \, / \, \text{numerical aperture}$$

Thus with increasing NA, the sin(illuminator) must increase to maintain a constant sigma value. Increasing illuminator angle decreases symmetry of the interference about the optical axis and this loss of symmetry induces a phase error in the presence of an aberration such as defocus. As figure 2 shows, increasing illuminator angle decreases DoF. Thus, due to the difference in illumination angle, it makes no sense to use 0.3 sigma at 0.45NA and 0.75NA. It is better to fix the illumination angle and let sigma change. For the 70nm node, we found that a good sigma would be 0.15. This is shown in Figure 3, which compares process windows at 0.15 and 0.25 sigma values for 45nm lines and 140nm pitch, and shows that the lower value, sigma of 0.15, is superior.

Weak PSM Illumination

Whereas the diffraction pattern of strong PSM has no zero order and requires on-axis illumination for proper imaging, weak PSM has zero order energy. Therefore, to get ideal two beam interference requires placing the source off the optical axis so that the diffraction pattern is tilted in such a way that zero and one of the first orders pass through the pupil at equal but opposite angles from the optical axis. To then design an ideal two-beam interference system for a given pitch, it is simple to calculate the angular spread between the centers of the zero and the first orders and divide by two. The ideal situation occurs only for point sources, which is not the case for typical state-of-the-art exposure tools that have some finite angular range defined by sigma. If you consider the convolved source with diffraction orders to represent an infinite set of coherently linked points with angular separation in sigma space of $\lambda(\text{Pitch} \cdot NA)^{-1}$ then there are many points that have non-equal interference angles relative to the optical axis. So in the case of interference during the strong PSM case, these asymmetries induce phase error with aberrations and imaging performance is lost.

Now for the case at hand, there are three general types of off-axis illuminators (OAI): the annulus, quadrupole, and dipole. Typically, they are "strong," meaning that there is no source energy between the poles, though they can be weak.[9, 10] For our cases the annulus would be too weak of a source because of the amount of non-optimal interference that arises from its shape. This leaves quadrupole placed at 45 degrees to the x- and y- optical axes or as a cross-quad placing the poles on the x- and y- axes, and the dipole, which has two poles on the x- or y-optical axis. Because of placing the poles at the 45-degree position, the smallest pitch that can be imaged is larger than for sources placed on the x- and y- axes. At extreme pitches, cross-quads[9] work best for contact holes and dipoles work best for line-space features. Table 1 shows the sigma value for pitches from 140nm to 220nm. Values equal to or greater than one will lose coherent linkage and will not image. Experience shows that the maximum sigma approximates:

$$\sigma_{\text{center}} \approx n \cdot \lambda \cdot (2 \cdot \text{pitch} \cdot NA \cdot (1 - \sigma_{\text{radius}}/2))^{-1}$$

where n=1 for dipole and cross-quad and n=√2 for quadrupole. So to image a 140nm pitch structure a center pole position of |0.92| to |0.97| should be optimal. Systems are just becoming available that have outer sigma values greater than 0.9. For this analysis, we will use 0.92 as the center sigma, with a pole radius of sigma equal to 0.12. For the 80nm, 180nm, and 200nm contacts we used a cross-quadrupole with center sigma of 0.70 and radial sigma of 0.1.

Resists

Resists need to have the correct contrast, low acid diffusion, optical properties and masking capability to provide the best performance for imaging 45nm and 70nm gates and 80nm contacts. Because there is a need to image pitches as small as 140nm it means that the resist contrast should be high so that a small imaging bias will allow the best sampling of the set of defocused aerial images. In addition, the resist should be insensitive to side-

lobe printing of contacts. Resist for 193nm are still evolving, but 248nm resists that have the right characteristics have the PROLITH lumped-parameter-model values of contrast equal to 23, diffusion of 4, and absorbance of 0.2 to 0.4. For this work we used contrast = 18.82, film thickness as specified (but typically 200nm), absorbance= 0.5 or 0.8, and aerial image diffusion length of 4nm.

The best weak phase-shift technique for the 70nm node uses a chromeless shifter-shutter technique, chromeless phase lithography (CPL). CPL, developed by ASML MaskTools, ASML, and PAL (as a contractor) tunes the diffraction pattern of a shifter-shutter structure with biasing and half-toning of chromeless phase-shifters and chrome sub-resolution assist features. This diffraction pattern is tuned to match that of another weak phase shifter whose transparency and phase shifting produces an optimal aerial image. Using biasing alone with no assist features or chrome structures can produce very good results for dense and semi-dense lines. Figure 4 shows the focus-exposure process window for ± 10% CD control. In this figure, 4a shows the process contours for 45nm lines on pitch of 140nm, 160nm, 180nm and 200nm, as well as 70nm lines on 140nm pitch. Figure 4b shows their individual exposure latitudes (EL) versus depth of focus (DoF) and figure 4c shows the EL vs. DoF for the common corridor and corresponds to the shaded area in figure 4a. These latitudes are large, but will need full CPL applied to the design so that the small features shown in Figure 4's table can be fabricated using half toning and so that the method can be extended to larger pitches. The one drawback is that dipole imaging only works for one orientation so the technique uses two or more exposures to build the pattern. This is not impossible and if a design feature set is limited to x- and y- orientations then the critical features can be broken into the two orientations and stitched together. The method of diffraction tuning is discussed elsewhere in this conference.[11]

Alternating Phase-Shift Masks for Topography for the 70nm Node

As stated earlier, done properly, alternating phase-shift technology is a strong phase-shifter imaging technique. However, it has several problems. First, it is difficult in some layouts to make assignments of phase to get the strong phase shift. Second, even if the assignment is made correctly, if the integrated energy of the opposed phase regions are not equal, zero order energy will not be null-ed and will contaminate the diffraction pattern. Third, bright field layouts give rise to strong shifted chromeless phase-edges (not weak PSM shifter-shutters) and they produce an unwanted artifact that must be trimmed with another exposure. Fourth, there are numerous three dimensional effects that reduce energy in the phase region and in addition, gives rise to a phase dependence on pitch. These topography problems degrade image quality and cause image placement focus dependent problems making placement the key process window limiter.[12, 13, 14] Thus, this fourth item truly limits the capability to produce across pitch solutions, and, makes solving the topographic problem critical for attaining the 70nm node and forces a discussion about fabrication options.

The two most promising mask-making techniques are the asymmetric bas (AsyBias) and the sidewall chrome alternating aperture (SCAA) mask. AsyBias makes the darker aperture brighter by making it bigger. The issue with this is that to make insensitive to wall angle an undercut etch would be used to move the quartz edge away from the active image formation region at the chrome edge but for these small features would make the mask structure unstable.[15] SCAA eliminates the problem by placing chrome at the top and bottom of the alternating apertures, thus no energy is lost and there is no wall profile dependence on phase. Figure 5 compares TE and TM polarization of AsyBias (5b) and SCAA (5a) for 45nm features on 140nm pitch whose wall angle varies from 75° to 89°. These TEMPESTpr results show that AsyBias has an extreme dependence on wall angle whereas SCAA has none in TE and amount that is less than that for AsyBias in TM. Due to AsyBias wall angle dependency; it probably is not a reasonable fabrication technique for the 70nm node. Note that this holds true for chromeless phase-edge masks too. This leaves SCAA. Figure 6 shows the phase dependence of SCAA without an anti-reflective coating (ARC) for a 45nm line. In this figure, a phase error of 1.4° is predicted by simulation. The error introduces zero order contamination that is described[12] by the ratio of zero order power to first order power, or $E^2_{zero} / E^2_{first-order}$. An ARC on top of the chrome is used during actual fabrication and based on work at 248nm exposure, should mitigate the phase problem.[12] Since this is not a mask fabrication paper, and realizing that work needs to be done to develop SCAA over the more traditional AsyBias if we are to use it (SCAA) at the 70nm node, we summarize the attributes of the two techniques in Figure 7 for reference.

Across Pitch Strong Phase-Shift Solutions

Now knowing that an across pitch mask fabrication technique exists, we will examine across pitch imaging solutions. For this study, biasing was used to find concurrent solutions for 140nm pitch with 45nm and 70nm g ates. Solutions were also found at other pitches (150nm, 160nm 180nm 200nm, 220nm, 240nm, 300nm, and 695nm) for

45nm lines. For each pitch in this study, a set of mask features varying line size was defined. Then the masks were simulated through a wide range of focus and exposure conditions with PROLITH, using the vector (unpolarized) image calculation mode, LPM resist model, and 193nm, 0.75NA / 0.15σ exposure setup. After exporting results to ProData™ (KLA-Tencor), the best common corridor solutions for 45nm and 70nm lines at 140nm pitch were found. Then, using those solutions, matches with the other pitches were sought, with the best ones shown in Figures 8 and 9. The low dose solutions are shown in Figure 8 and the high dose in Figure 9. Each figure contains a table that shows the target CD, pitch, normalized-image-log-slope (NILS), DoF, dose-to-size (E_{size}) and nominal dose for the focus-exposure (FE) range. The nominal dose equates to the dose that samples the best process window within ±10% CD control. For low dose, overlapping solutions are found for the pitches 200nm and below at a dose of 2.14 E0, with a common DoF of 0.29μm and 5% EL.

The high dose solution shown in Figure 9 was restricted to 140nm, 160nm (design-rule exception), 220nm, 240nm, 300nm and 695nm and has a common DoF of 0.36μm with 5% EL at a dose of 5.12 E_0. This does not mean that solutions could not be found for 180nm and 200nm pitches, but the positive biasing exceeded our minimum at 1X feature width of 60nm. For instance, the 160nm pitch results in Figure 9 were produced with a 106nm line-54nm space (1X) that failed this criteria but provided a solution. With continued fabrication improvements, more solutions will become available. Next, we will examine device-like structures.

<div align="center">Device-like features</div>

In this section, we will be using dark field alternating PSM plus trim exposure to make two-dimensional features. In the previous section, we looked at infinitely long and repeating features. As long as the alternating apertures produce, the same, integrated amount of energy the zero order would be nulled and we would only detect higher diffraction orders. The two dimensional problem is more complex because the zero order energy may arise from other contributing features such as non-y oriented features when studying diffraction on the σ_x-axis or from loss of energy due to diffraction at the corner of the alternating apertures. The way to solve this problem is to perturb features in different orientations and compare results to features that have been isolated from other orientations. The responses we monitor are diffraction pattern amplitude of first and zero order, focus-exposure responses to each critical CD, and image placement. The exact detail of this method is beyond the scope of this work and we will now move to examples of 6 transistor (6T) SRAM, 4 transistor (4T) and 2 transistor (2T) device-like features.

Figure 10 shows a dark field alternating 6T mask (10a), diffraction pattern (10b), aerial image (10c) and resist pattern (10d) prior to correction. The PROLITH illumination conditions were 193nm, 0.75NA, and 0.25σ. A_1/A_0 refers to the ratio of first order to zero order and is 0.192/0.172 = 1.13. This pattern is not strong phase-shifted. In the aerial image it appears as an imbalance in region A and B intensities, where $0.41 \leq A \leq 0.49$ and $0.83 \leq B \leq 0.91$. In the resist, fluctuations in the electric field show severe variation in the line-width. These fluctuations are caused by apertures that are too small for the design. By increasing the aperture sizes as shown in Figure 11 we were able to improve the strength of the phase-shift. Now $A_1/A_0 = 0.256 / 0.061 = 4.2$. Regions A and B are more similar in intensity, with $0.87 \leq A \leq 0.98$ and $0.76 \leq B \leq 0.87$ on the upper transistors. However, there are hotspots at the corners and in the A region of the lower transistors that still need corrections. Along with biasing, we use hanging and flying serifs to provide corner correction and correction to intensity ringing that arises from the use of low sigma.

While more corrections can be made, there is enough difference in the two layouts to compare their process windows. This is shown in Figure 12, where the line width is sampled at the mid-point of active for four of the SRAM transistors and one of two wordlines. The uncorrected case has no common corridor and the corrected case has a small 0.19nm DoF at 5% EL. Note that the DoF is small because we are not complete with the correction and because of using sigma of 0.25, which was chosen to model the illumination that is available today.

In the next example, we show some of the other corrections that we make as well as what the pattern looks like in resist during each individual exposure and after both. Figure 13 shows a 4T example where we applied exterior phased assist features that when wrapped on the mask pitch provides a feature in size equal to the opposing phased aperture. Being on pitch with the critical features is always optimal but may not always be possible as in this case. Further, to improve performance we will run a chrome half-tone structure down the middle of the center space to reduce the brightness of this space. To do this properly the pitch of the half tone structure needs to be small enough to diffract the higher orders out of the lens. In the same fashion as the previous figure, a typical correction for a 2T pattern is shown in Figure 14. Again, we have found using assist features of opposing phase yields the best

electric field balance. In those cases, the best result would be to make an infinite series of lines and spaces of approximately seven or eight lines and then trim out the unwanted features during the other exposure. However, if real estate is limited, set the assists to have an effective linewidth equal to half of the primary space of opposing phase. This will null the field.[16]

<div align="center">Brief Look at Contacts</div>

Contacts have become the technology driver for sub-140nm imaging. For the 70nm node, we evaluated 80nm contacts on a 180nm pitch. Our current solution uses an attenuated PSM with 15% transmission. For illumination, as previously mentioned, we used a cross-quadrupole with center sigma of 0.7 and radial sigma of 0.1. Figure 15 shows the mask, (15a) the diffraction pattern convolved with the source (15b), the NILS through focus (15c), and the %EL versus DoF for the 180nm pitch. The NILS are less than one suggesting poor exposure latitude but the values also do not vary too much with focus suggesting good DoF and that is observed in the focus-exposure simulation. The latitude hovers above 5%EL over a focus range of 0.68μm. Better solutions need to be sought and that is the subject of ongoing work.

<div align="center">Conclusion</div>

Two beam imaging techniques using strong and weak phase-shift mask (with off-axis illumination) were shown. Due to affects caused by mask topography, it was shown that SCAA masks would work better for the 70nm node than the more conventional AsyBias mask. Whichever strong shift mask is used; it was shown to maintain the same degree of phase-shift imaging strength that a sigma in the range of 0.15 will be optimal. Such a low sigma is not currently available and barring any engineering limitations needs to be developed. In addition, to using SCAA and low sigma, it is advantageous to use optimal pitch gratings during the dark field altPSM exposure and then remove the unwanted patterns during the trim exposure as we showed with 4T and 2T examples and has been discussed by Fritze et al[3]. For weak PSM, CPL with dipole was shown to be a good choice for 0.75 NA, but to minimize the number of exposures per layer; it would be advantageous to use tools with larger NA so that quadrupole illumination would be useable. Finally, it was shown that using current attenuated PSM technology with cross-quadrupole illumination 80nm contacts on a 180nm pitch can be imaged; however, the process will not be robust and better solutions need to be developed.

<div align="center">Acknowledgement</div>

Figure 1: 120 nm Line, 240 nm Pitch DoF versus NA for Different Sigma
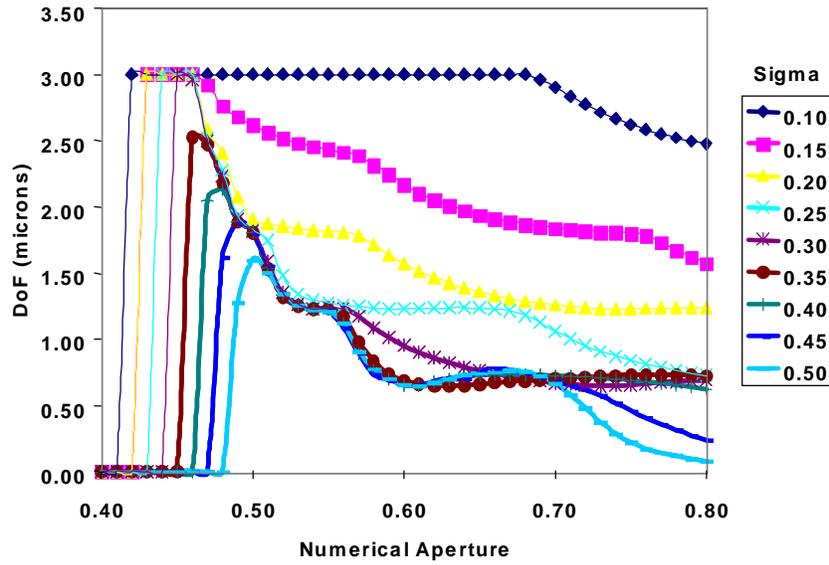
Figure 2: 2120 nm Line, 240 nm Pitch DoF versus sin(Illuminator) for NA

NA	Sigma	sin(Ill)	DoF
0.45	0.30	0.14	3.00
0.50	0.30	0.15	1.81
0.55	0.30	0.17	1.24
0.60	0.30	0.18	0.95
0.65	0.30	0.20	0.77
0.70	0.30	0.21	0.67
0.75	0.30	0.23	0.66
0.80	0.30	0.24	0.69
0.75	0.15	0.11	1.80
0.75	0.20	0.15	1.23
0.75	0.25	0.19	0.84
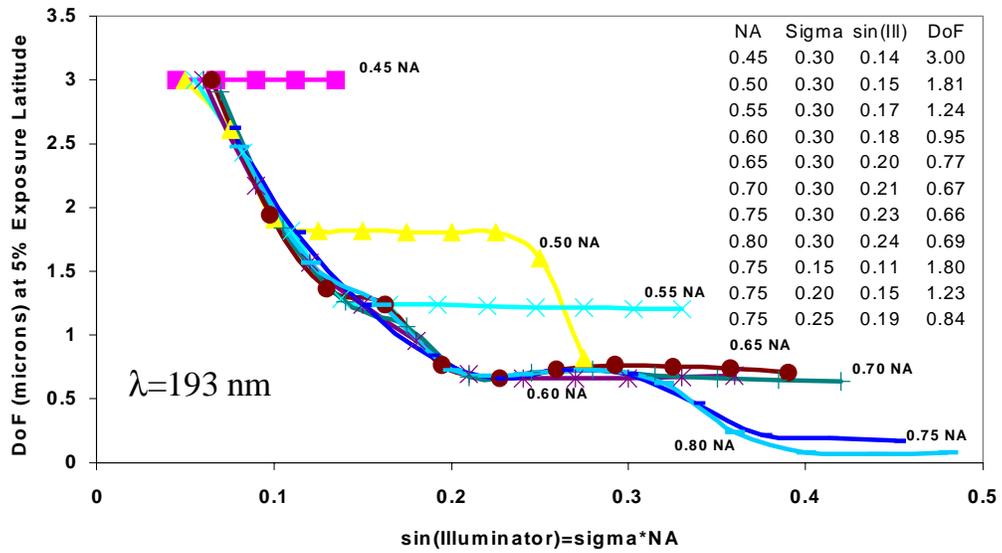
λ=193 nm

Figure 3: DoF and % EL Depedence on Sigma for 70nm Line:Space 193nm/0.75 NA

Legend:
- Sigma 0.15 has 1.03μm DoF
- Sigma 0.25 has 0.80μm DoF
- Sigma 0.35 has 0.00μm DoF

LPM Parameters
Contrast =18
Film Thickness = 200nm
Diffusion=4nm
Rmin = 0.00 nm/s

Y-axis: Exposure Latitude (%)
X-axis: DoF(μm)
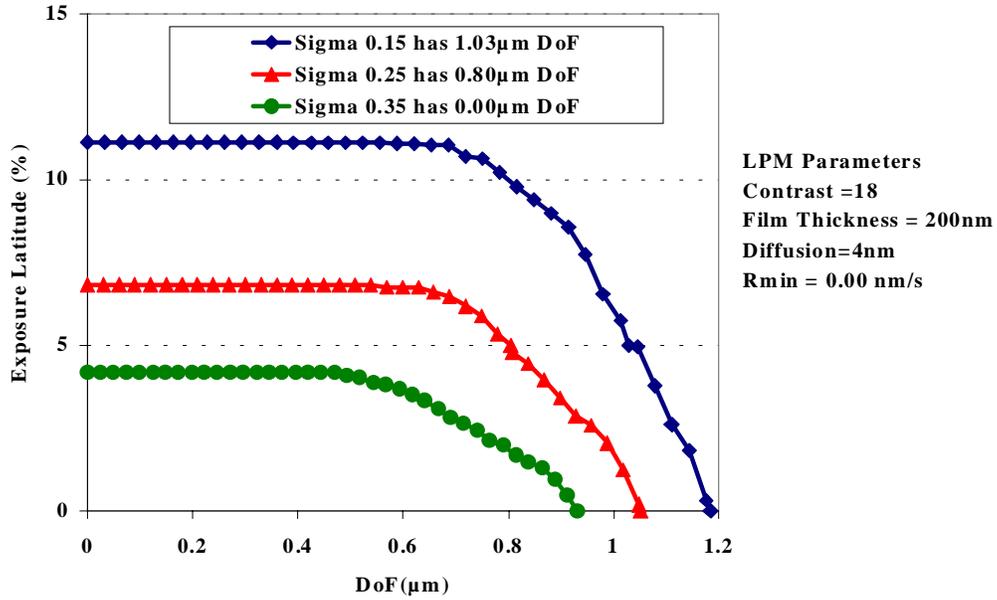
Table 1: Off-axis for Weak PSM

For 0.75 NA, 193nm Exposure		
Pitch	Dipole σ	Quad σ
140	0.92	1.30
150	0.86	1.21
160	0.80	1.14
170	0.76	1.07
180	0.71	1.01
190	0.68	0.96
200	0.64	0.91
210	0.61	0.87
220	0.58	0.83

Figure 4: CPL PROLITH Results for 45nm lines on pitches of 140nm, 160nm, 180nm and 200nm and a 70nm line on a 140nm pitch.

(a)

(b)

(c)

0.33μm DoF

Pitch (nm)	Target (nm)	Mask (nm) (1X)	NILS	DOF (μm)	Esize (E0)	Nominal (E0)
140	45	23	1.9	1.16	1.55	1.55
140	70	60	1.41	0.81	1.55	1.55
160	45	23	1.49	0.6	1.55	1.55
180	45	28	1.45	0.43	1.55	1.55
200	45	28	1.01	0.32	1.55	1.55

193 nm
0.75 NA
Dipole
σ_{Center}=0.92
σ_{Radial}=0.12
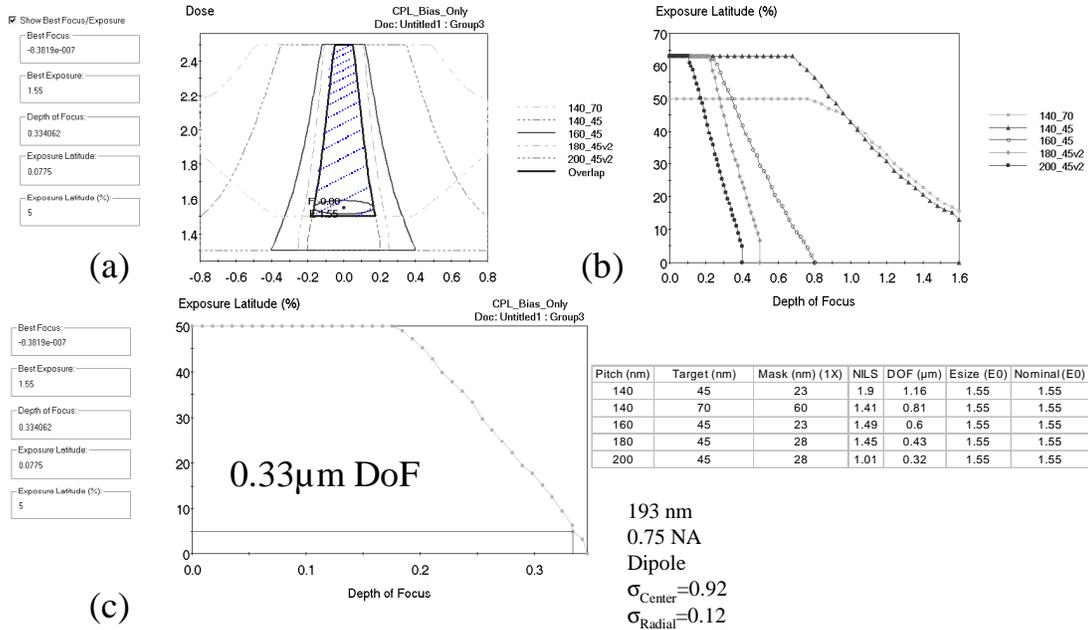
Figure 5: TE and TM Electromagnetic field simulation of 140nm pitch with an effective line size of 70nm and wall profiles varied from 75 to 89 Degrees.

SCAA   AsyBias

TE

TM

Simulation Grid x=z=3nm
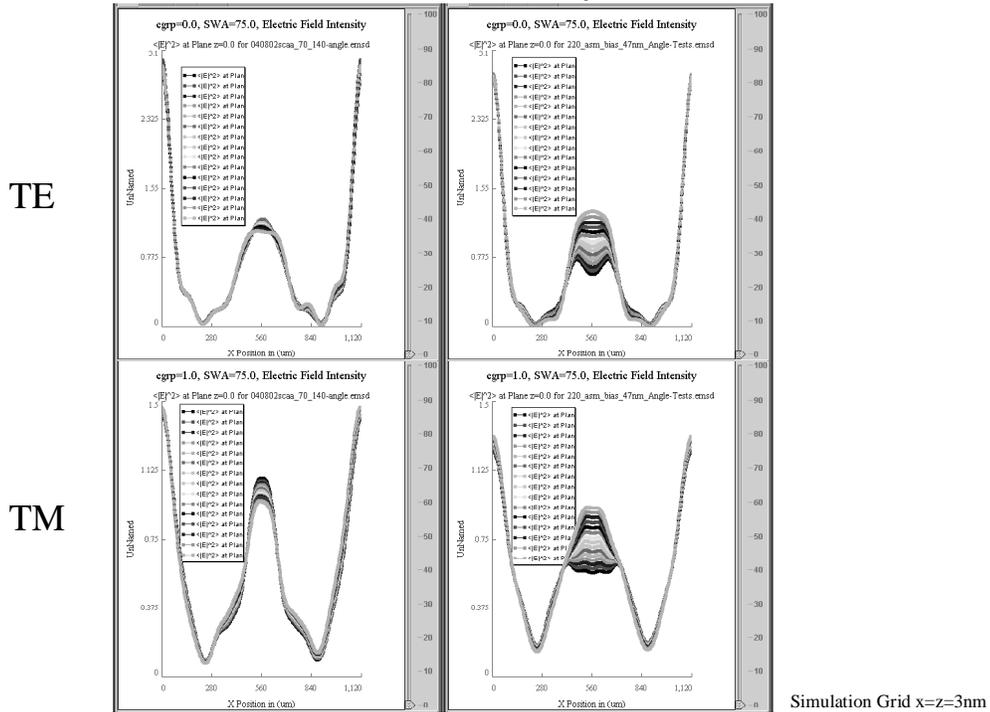
Figure 6: Phase error and power of 45nm Lines (no ARC on Mask) on a pitches from 140nm to 300nm.
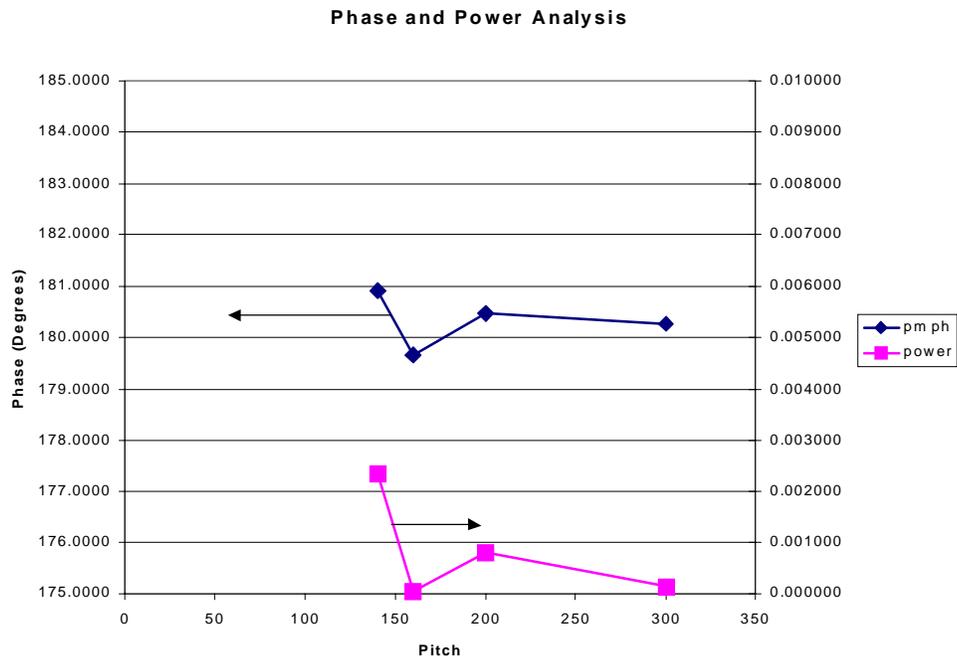
Figure 7: AltPSM Issue Comparison

Figure 8: AltPSM Low Dose Solutions

Case number	Target	Line Size (nm)	Pitch (nm)	NILS	DOF (µm)	Esize (E0)	Nominal Dose (FE) (E0)
case024_45	45nm	65	140	0.917	0.702	2.180	2.139
case026_70	70nm	75	140	1.311	1.051	2.155	2.231
case055_45	45nm	70	150	1.343	0.427	2.129	2.058
case070_45	45nm	70	160	1.443	0.427	2.218	2.133
case080_45	45nm	70	180	1.584	0.444	2.129	2.028
case090_45	45nm	70	200	1.680	0.451	2.180	2.064

Show Best Focus/Exposure

Best Focus:
2.6457e-005

Best Exposure:
2.14378

Depth of Focus:
0.289889

Exposure Latitude:
0.107189

Exposure Latitude (%):
5

Predict 0.29 µm DoF

Dose

F 0.00
E 2.14

case024_45
case026_70
case055_45
case070_45
case080_45
case090_45
Overlap

Focus
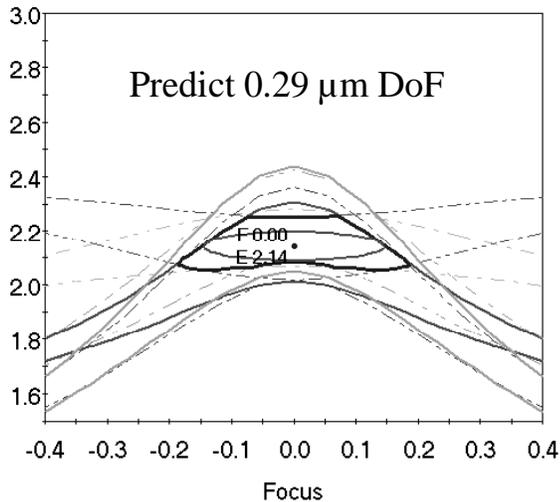
Figure 9: AltPSM High Dose Solutions

Case number	Target CD	Line Size (nm)	Scatter Bar (nm)	Pitch (nm)	NILS	DOF (µm)	Esize (E0)	Nominal Dose (FE) (E0)
Case030_45	45nm	95	0	140	0.92	0.70	5.17	5.08
Case031_70	70nm	100	0	140	1.31	1.05	5.08	5.26
Special Case 160nm	45nm	106	0	160	1.44	0.35	5.19	5.12
case124_45	45nm	115	0	220	1.75	0.45	5.37	5.05
case142_45	45nm	110	0	240	1.80	0.45	5.20	4.92
case156_45	45nm	75	0	300	1.90	0.45	5.37	5.03
p695xCase008_45	45nm	70	60	695	1.88	1.07	5.16	4.99
p695xCase046_45	45nm	70	80	695	1.89	0.55	5.30	4.95

DOF and EL Selections:
DOF 0.35 um EL 5.00 %

Show Best Focus/Exposure

Best Focus:
3.75807e-005

Best Exposure:
5.12061

Depth of Focus:
0.347639

Exposure Latitude:
0.256031

Exposure Latitude (%):
5

F 0.00
E 5.12

case030_45
case031_70
case124_4b
case142_45
case156_45
p695_SBmasks_008_45
Special 160nm Pitch Case
Overlap

Focus
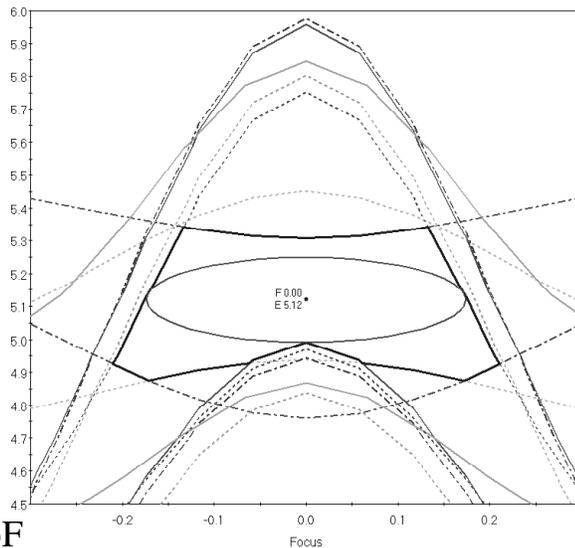
Predict 0.35 µm DoF

Figure 10: Uncorrected of dark field altPSM 6T SRAM (Case s45_r2)), (a) dark field altPSM; (b) diffraction pattern convolved with the source; (c) altPSM plus trim aerial image; (d) resist pattern overlayed with altPSM.

(b)

A1/A0=1.13

0.194

0.172

Region A

Region B

(a)

(c)

(d)
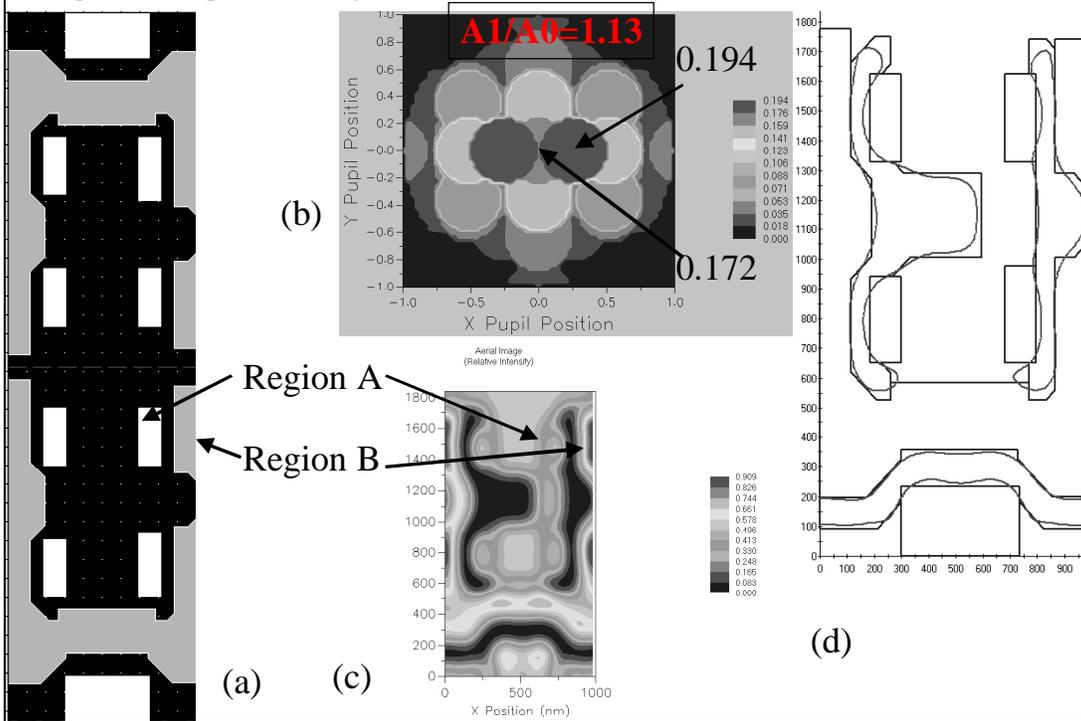
Figure 11: Partial Correction of dark field altPSM 6T SRAM (Case sa_g45_r91), (a) dark field altPSM; (b) diffraction pattern convolved with the source; (c) altPSM plus trim aerial image; (d) resist pattern overlayed with altPSM.

(b)

A1/A0=4.2

0.256

0.061

Region A

Region B

(a)

(c)

(d)
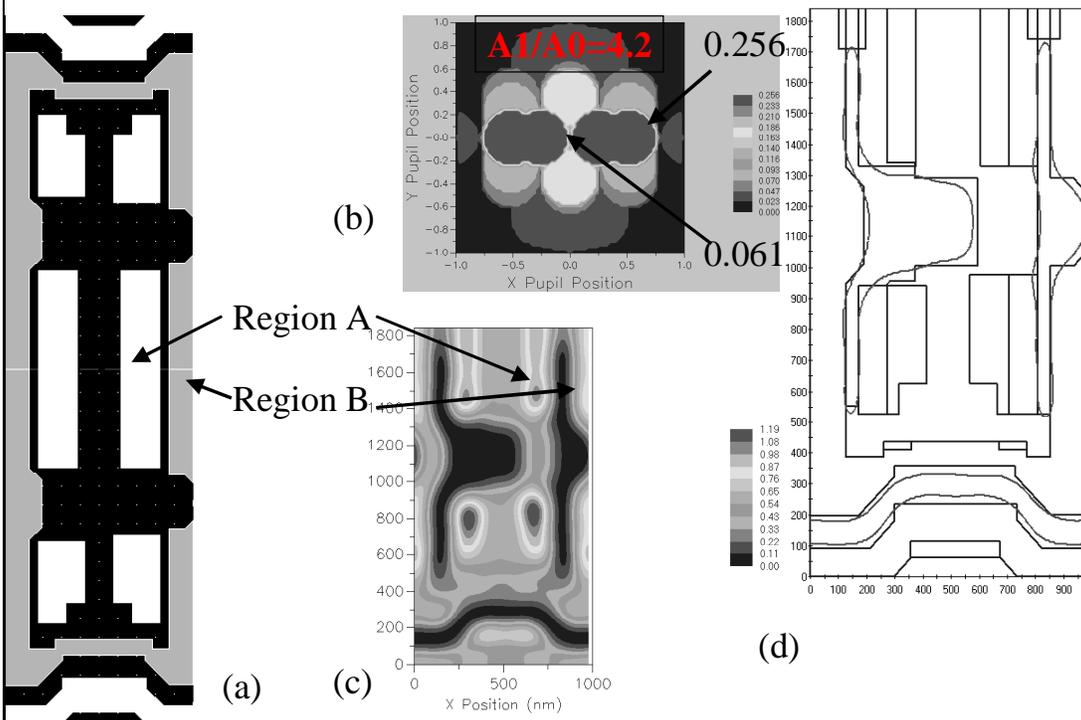
Figure 12: Process window for each unique transistor Uncorrected and Corrected SRAM.
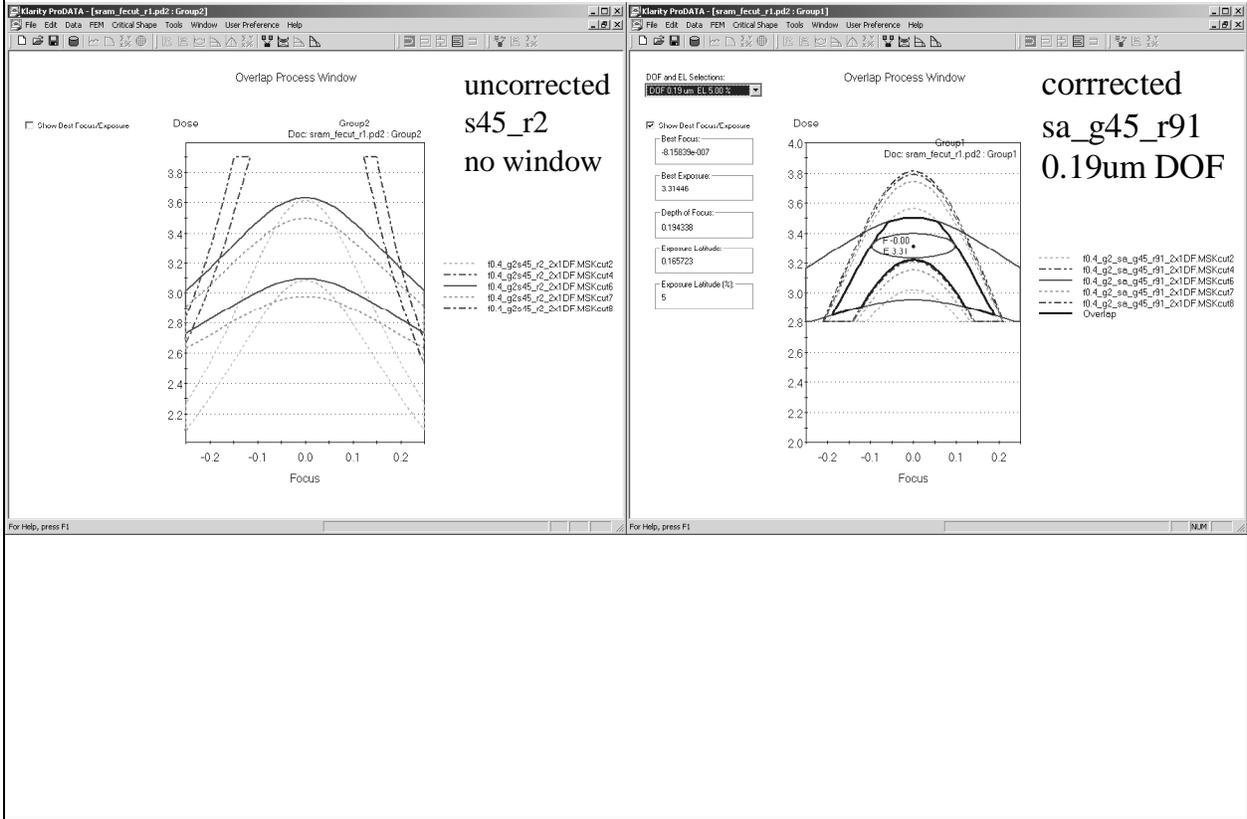
Figure 13: 4T Dark Field altPSM+Trim, top row shows, from left to right, dark field trim mask, bright field trim mask, and the target design. The bottom row shows the respective resist image for each mask pattern, with the resist outline overlayed on the altPSM at the far right, bottom.
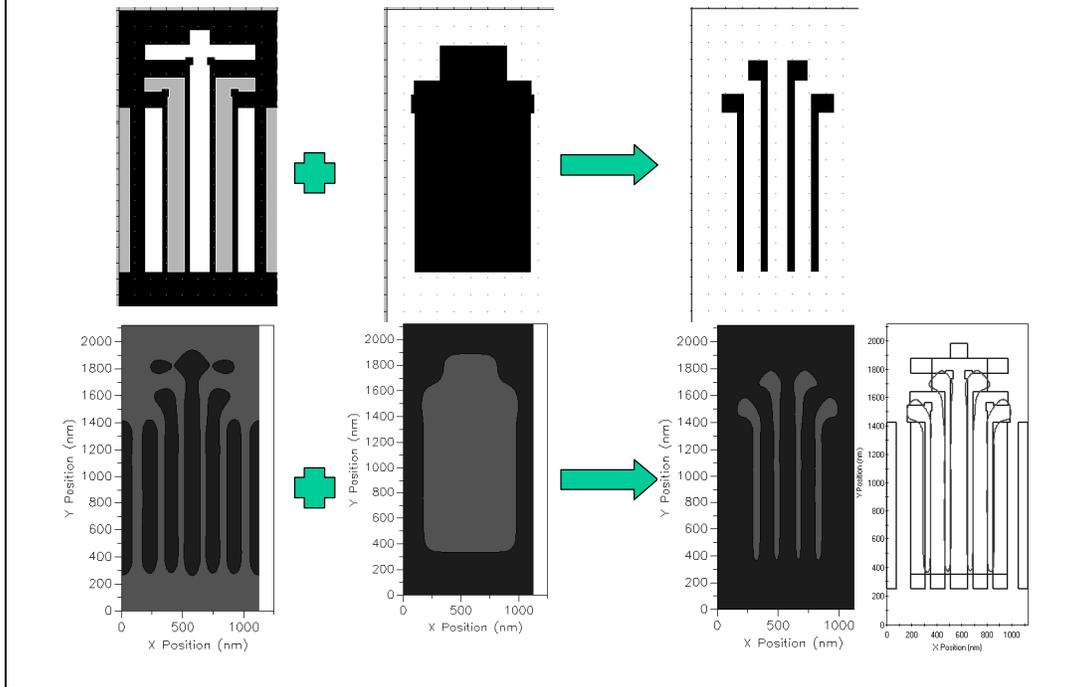
Figure 14: 2T example, top row shows, from left to right, dark field trim mask, bright field trim mask, and the target design. The bottom row shows the respective resist image for each mask pattern, with the resist outline overlayed on the altPSM at the far right, bottom.
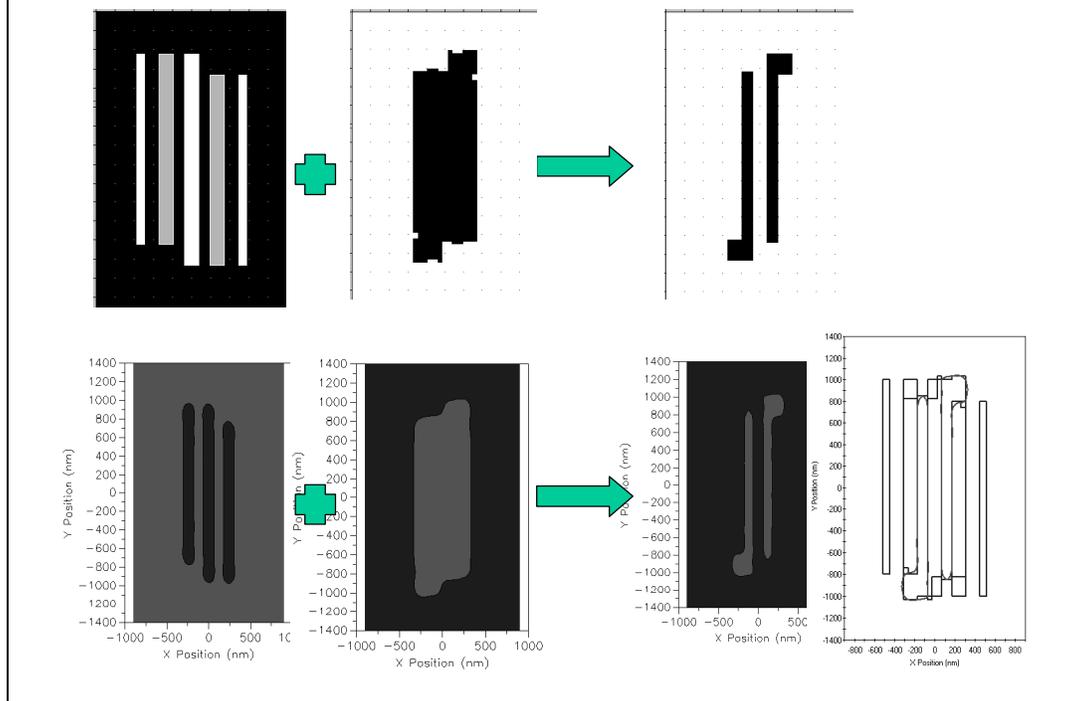
Figure 15: Image simulation of 15%attenuated PSM 80nm on 180nm pitch result. Going clockwise from upper left, (a) the mask; (b) the diffraction pattern convolved with the cross-quadrupole source; (c) NILS dependence on focus; (d) percent exposure latitude with respect to DoF.
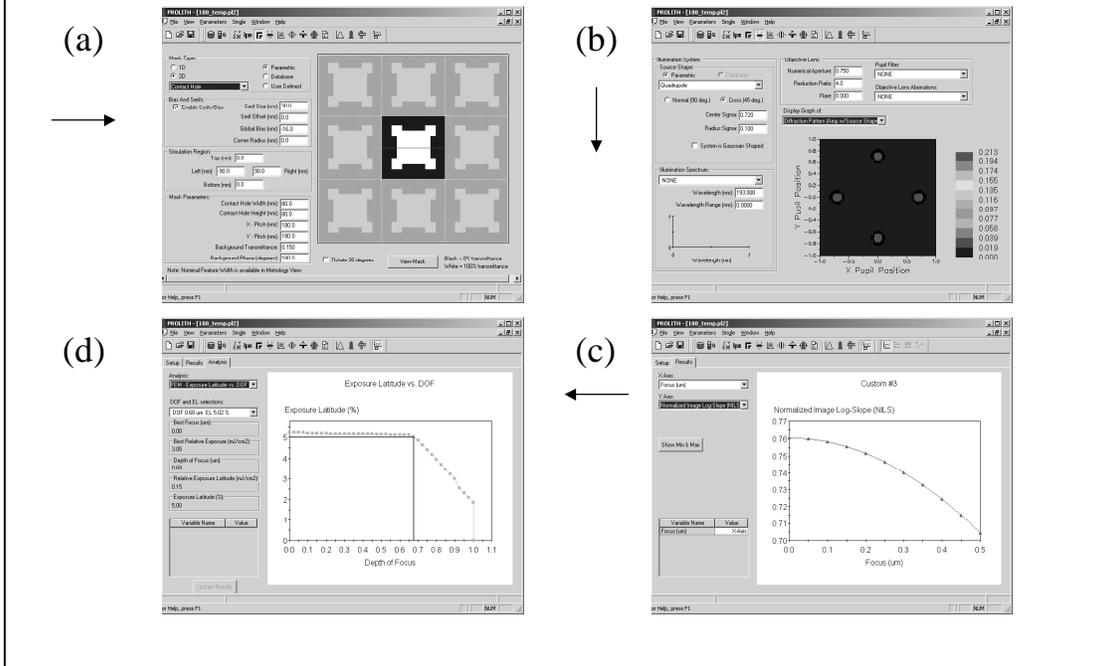
References

[1] H-Y Liu, L. Karklin, Y-T Wang and Y. C. Pati, SPIE 3236, pp. 328-337 (1997).

[2] M. E. Kling, N. Cave, B. J. Falch, C-C Fu, K. Green, K. D. Lucas, B. J. Roman, A. Reich, J. L. Sturtevant, R. Tian, D. Russell, l. Karklin and Y-T Wang, SPIE 3679, pp 10-17 (1999).

[3] M. Fritze, B. Tyrrell, D. Astolfi, D. Yost, B. Wheeler, R. Mallen, J. Jarmolowicz, S. Cann, H-Y Liu, M. Ma, D. Chan, P. Rhyins, C. Carney, J. Ferri, B. A. Blachowiez, SPIE 4346, pp. 191-204 (2001).

[4] J. Fung Chen, J. S. Petersen, R. Socha, T. Laidig, K. E. Wampler, K. Nakagawa, G. Hughes, S. MacDonald, W. Ng, SPIE 4346, pp. 515-533 (2000).

[5] M. D. Levenson, Physics Today, pp. 28-36, (July, 1993).

[6] C. A. Mack, Interface '91, pp. 23-35 (1991). (Described in Edge Superposition section, p.27)

[7] S. K. Kim, J. G. Hong, J. O. Park, T. J. Yoo, Y. S. Hyun, C. K. Bok and K. S. Shin, SPIE 4346, pp. 214-228 (2001).

[8] J. S. Petersen, M. McCallum, N. Kachwala, R. J. Socha, J. Fung Chen, T. Laidig, B. W. Smith, R. Gordon, C. A. Mack, SPIE 3546, pp. 288-303 (1998).

[9] B. W. Smith, L. Zavyalova, J. S. Petersen, SPIE 3334, pp. 384-394.

[10] B. W. Smith, SPIE 4346, pp. 471-485 (2001).

[11] J. S. Petersen et al., SPIE Conference 4692 paper 68.

[12] R. A. Ferguson, A. K. Wong, T. A. Brunner, L. W. Liebmann, SPIE 2440, pp.349-360 (1995).

[13] J. S. Petersen, R. J. Socha, A. Naderi, C. Baker, S. Rizvi, D. VanDenBroeeke, N. Kachwala, F. Chen, T. Laidig, K. E. Wampler, R. Caldwell, S. Takeuchi, Y. Yamada, T. Senoh, M. McCallum, SPIE 3412, pp. 503-520 (1998).

[14] D. J. Gerold, J. S. Petersen and M. D. Levenson, SPIE 4346, pp. 729-743 (2001).

[15] C. E. Tabery and C. A. Spence, SPIE 4346, pp. 429-440 (2001).

[16] J. S. Petersen, SPIE 4000, pp. 77-89 (2000).